SCIENCE CHINA
Earth Sciences

•ARTICLE•

August 2023 Vol.66 No.8: 1877–1891
https://doi.org/10.1007/s11430-022-1106-4

A Paleozoic mercury mineralisation event in South China: *In situ* U-Pb dating and chemical compositions of calcite from the Jianyan Hg deposit

Kai LUO[1,2], Jiaxi ZHOU[1,2,3*], Alexandre CUGERONE[4], Meifu ZHOU[3†], Yuexing FENG[5], Zhongguo JIN[6] & Jianxin ZHAO[2]

[1] *Key Laboratory of Critical Minerals Metallogeny in Universities of Yunnan Province, School of Earth Sciences, Yunnan University, Kunming 650500, China;*
[2] *School of Earth and Environmental Sciences, The University of Queensland, Brisbane QLD 4072, Australia;*
[3] *State Key Laboratory of Ore Deposit Geochemistry, Institute of Geochemistry, Chinese Academy of Sciences, Guiyang 550081, China;*
[4] *Department of Earth Sciences, University of Geneva, Geneva 1205, Switzerland;*
[5] *Southern Marine Science and Engineering Guangdong Laboratory, Zhuhai 519000, China;*
[6] *Non-Ferrous Metals and Nuclear Industry Geological Exploration Bureau of Guizhou, Guiyang 550005, China*

Received October 31, 2022; revised March 8, 2023; accepted April 17, 2023; published online July 19, 2023

Abstract The ages of hydrothermal Hg deposits are difficult to constrain because of the lack of suitable minerals for dating. The South China low-temperature metallogenic domain hosts numerous Hg deposits, including the Jianyan Hg deposit that is composed mainly of cinnabar and calcite. There are two stages of calcite in the deposit: syn-ore calcite (Cal-I) and post-ore/barren calcite (Cal-II). Cal-I is mainly euhedral-subhedral and fine-grained, has homogeneous grey luminescence, and is associated with cinnabar. Subhedral-anhedral Cal-II crosscuts Cal-I and is relatively coarse-grained. The syn-ore Cal-I has high U contents (0.1–1.3 ppm) and U/Pb ratios (up to 4.2), and is thus suitable for U-Pb dating. Using a laser ablation-inductively coupled plasma-mass spectrometer equipped with ion counters, we obtained a U-Pb age of 426.3±5.7 Ma (MSWD=1.5) for Cal-I. This age is interpreted to represent the timing of Hg mineralisation at Jianyan and is similar to ages of 440–400 Ma reported for many carbonate-hosted Pb-Zn and Ba-F deposits in South China. Based on the present results in combination with existing geochemical and geochronological data, we infer that these deposits belong to a Paleozoic Hg-Pb-Zn-Ba-F mineralisation system that was controlled by Caledonian tectonism.

Keywords *In situ* calcite U-Pb dating, Paleozoic Hg mineralisation, Caledonian tectonism, Jianyan Hg deposit, South China

Citation: Luo K, Zhou J, Cugerone A, Zhou M, Feng Y, Jin Z, Zhao J. 2023. A Paleozoic mercury mineralisation event in South China: *In situ* U-Pb dating and chemical compositions of calcite from the Jianyan Hg deposit. Science China Earth Sciences, 66(8): 1877–1891, https://doi.org/10.1007/s11430-022-1106-4

1. Introduction

Low-temperature mineralization (generally <200–250°C), has occurred in South China and the midwestern United States, is characterized by numerous epigenetic hydrothermal deposits (Tu et al., 2004). However, the timing of low-temperature mineralization is difficult to constrain because of the lack of minerals suitable for dating (Leach et al., 2001; Cline et al., 2005). In South China, low-temperature mineral deposits are distributed over an area of ~500,000 km^2, forming the South China low-temperature metallogenic domain and accounting for >50% of global reserves of Sb, 10% of Au, 9% of Hg, and 5% of Pb+Zn

* Corresponding author (email: zhoujiaxi@ynu.edu.cn)
† Corresponding author (email: zhoumeifu@hotmail.com)

(Peng et al., 2003a; Hu et al., 2017). These deposits include carbonate-hosted Hg, Pb-Zn, and Ba-F deposits; Carlin-type Hg-Au-As-Sb deposits; and vein-type Au-Sb deposits (Figure 1; Wang et al., 2020; Zou et al., 2022). They are mostly hosted in sedimentary rocks, controlled by folds, faults, and lithological contacts, and generally formed during two main periods at 230–200 and 160–130 Ma, corresponding to the Indosinian (Triassic) and Yanshanian (Jurassic-Cretaceous), respectively (Figure 1; Su et al., 2009; Mao et al., 2013; Hu et al., 2017; Zhou et al., 2018). Older ages of 470–370 Ma have been reported for several deposits, but the geological significance of these ages is debated (Peng et al., 2003a; Hu et al., 2007; Zhang et al., 2018).

Epigenetic carbonate-hosted Hg, Pb-Zn, and Ba-F deposits in the south-eastern part of the Yangtze Block form a NW-SE-trending belt (i.e., the western Hunan-eastern Guizhou (WHEG) Hg polymetallic metallogenic belt) that is 150 km long and 5–10 km wide. The belt contains 72 Hg, ~300 Pb-Zn, and ~300 Ba-F deposits. Representative examples include the Wanshan Hg, Huayuan Pb-Zn, and Dazhuyuan Ba-F deposits (Figure 1; Wang et al., 2010; Hu et al., 2017; Zou et al., 2022). These deposits are poorly dated because of the simple mineral paragenesis comprising sulphides associated with calcite/dolomite, barite, fluorite, and rare quartz, and because of the low contents of radiogenic elements (Studemeister, 1984; Luo et al., 2020). Reported ages include a Rb-Sr age of 431±24 Ma for sphalerite from the Aozigang Pb-Zn deposit (Cao et al., 2015), Sm-Nd age of 364±24 Ma for calcite from the Luanyantang Hg deposit (Wang and Wen, 2015), and Rb-Sr age of 492±37 Ma for fluid inclusions hosted in quartz from the Pingqiu Au deposit (Hu et al., 2007). However, these dating methods have limited application due to: (1) the lack of good petrographic constraints with the presence of multiple stages of calcite and sphalerite mineralization as well as the occurrence of secondary fluid inclusion assemblages in quartz (Uysal et al., 2007; Su et al., 2009; Zhu et al., 2017); (2) the large errors and variations of ages within a single deposit (Liao et al., 2015; Yang et al., 2016), which might reflect a narrow range of Sm/Nd ratios or partial or total resetting of the isotopic systems by post-mineralisation hydrothermal fluids (Zhu et al., 2017; Luo et al., 2020); and (3) the presence of Rb-Sr-bearing clays in the dated minerals (Bradley and Leach, 2003).

Carbonate minerals can be dated *in situ* using U-Pb isotopes, which constrains the timing of mineralisation and tectono-metamorphic events associated with fluid-related U mobility (Luo et al., 2020; Pinet et al., 2022). This approach, employing laser ablation multi-collector inductively coupled plasma mass spectrometry (LA-MC-ICP-MS), can identify a wide range of U/Pb ratios at sub-millimetre scales due to its high spatial resolution (<100 μm) and low detection limits (~1 ppb Pb) (Nuriel et al., 2017). Previous studies have dated carbonates from Sb deposits (Luo et al., 2020; Xu et al., 2022), Pb-Zn deposits (Sheng et al., 2022; Xiong et al., 2022; Giorno et al., 2022), and Carlin-type Au deposits (Jin et al., 2021), but rarely from Hg deposits.

The Jianyan Hg deposit occurs in the WHEG carbonate-hosted Hg polymetallic mineralisation belt in the south-eastern Yangtze Block, and is the only Hg deposit still under exploration. In this paper, we report the results of *in situ* U-Pb dating of carbonate minerals in this deposit, and also mineralogical, compositional and Sr isotope analyses of syn-ore calcite. These results are compared with those from previous studies conducted elsewhere in the South China low-temperature metallogenic domain. Our data provide new insights into low-temperature mineralisation events in South China and clearly demonstrate a Paleozoic Hg mineralization event.

2. Regional geology

The South China Block is composed of the Yangtze Block to the northwest and the Cathaysia Block to the southeast, which was amalgamated along the Jiangnan Orogen at *ca.* 830 Ma (Figure 1; Zhao et al., 2011). The basement of the Yangtze Block includes late Archaean metamorphic rocks in the north, and late Paleoproterozoic to Neoproterozoic weakly metamorphosed rocks in the west and east. This basement has been intruded by widespread Neoproterozoic igneous rocks (Chen et al., 1991; Zhou et al., 2002; Wang et al., 2007). The basement of the Yangtze Block is overlain by a sedimentary succession that consists mainly of Cambrian-Triassic marine sedimentary rocks and Jurassic, Cretaceous, and Cenozoic continental sedimentary rocks (Yan et al., 2003).

The south-eastern margin of the Yangtze Block, where the carbonate-hosted Hg polymetallic deposits are located, experienced Late Proterozoic (820–635 Ma) extension and evolved in a passive continental margin setting during the early Cambrian (635–488 Ma; Li et al., 2003). The NE-SW-trending Baojing-Tongren-Yuping (BTY) fault divides a thick dolostone sequence to the west from bedded sandstone, mudstone, limestone, and dolostone to the east (Figure 1). In this area, an intra-continental orogeny began in the late early Palaeozoic (488–420 Ma), resulting in uplift and thus a lack of Late Ordovician-Jurassic sedimentary rocks (Zhang et al., 2019). Caledonian magmatic rocks were generated as a result of collapse of the late early Paleozoic orogen (Chu et al., 2012). These intrusions are located mainly on the south-eastern side of the Jiangnan Orogenic Belt (Figure 1). The early Mesozoic intracontinental orogeny (225–215 Ma) was likely due to the far-field effects of subduction of the Palaeo-Pacific Plate beneath the south-eastern margin of the South China Block (Chu et al., 2012).

NE-SW-trending faults and secondary E-W-trending folds

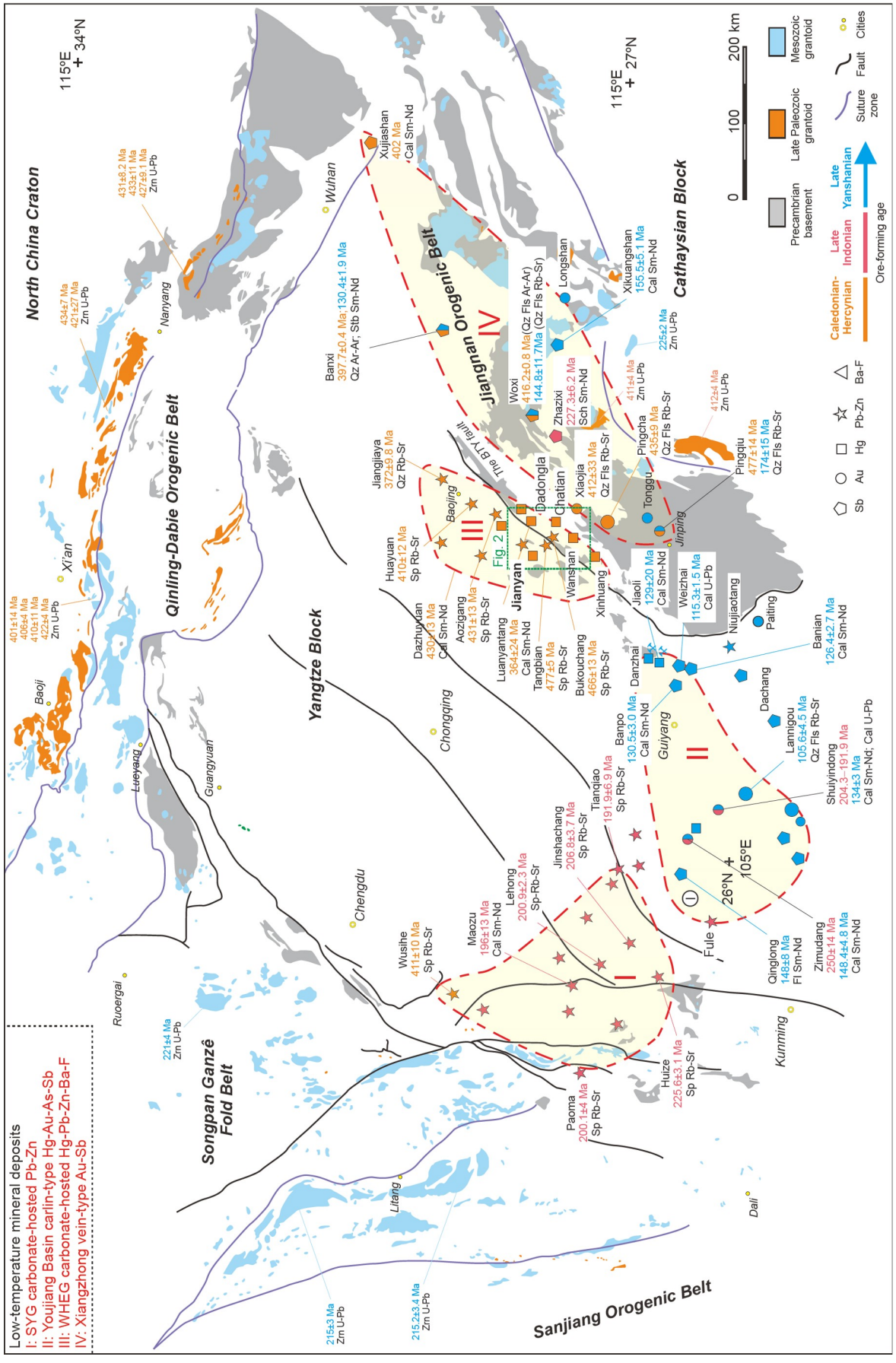

Figure 1 Simplified tectonic map of the Yangtze block and adjacent orogenic belts with granitoid rocks and metamorphic basement rocks, showing the South China low-temperature mineralisation domain that comprises four main mineralisation belts. The isotopic ages of mineral deposits of previous studies are listed in Appendix 1 (https://link.springer.com). The ages of granitoid rocks are from Li Y Q et al. (2018) and references therein. Abbreviations: Sp, sphalerite; Fl, fluorite; Cal, calcite; Apy, arsenopyrite; Qz, quartz; Py, pyrite; Stb, stibnite; Zm, zircon; Rut, rutile; Sch, scheelite.

in the study area record multiple phases of tectonic activity. The NE-SW faults are the main control on the spatial distribution of Hg deposits (Figure 2). The Hg mineralisation was also affected by bedding-parallel faults and is locally concentrated within fold axes and hinges.

3. Ore deposit geology

In the south-eastern Yangtze Block, carbonate-hosted Hg deposits are Hg-only deposits or related to Pb-Zn mineralisation, with Zn ore zones being better developed close to mineralisation along faults, such as the Chashula, Chatian, and Dadongla Hg-Pb-Zn deposits (Figure 1; Liu et al., 2017). These deposits may also contain Ba-F mineralisation and are generally hosted in Cambrian to Ordovician carbonate rocks. The deposits with large tonnages of ore (>2000 t Hg) are located mainly in the south-eastern parts of the Hg-Pb-Zn-Ba-F polymetallic mineralisation belt. Those with smaller tonnages (<500 t Hg) are located in the north (Wang et al., 2012).

Ore bodies of the Jianyan deposit are structurally controlled by the Shuiyinchang compressional NE-SW fault zone that comprises several reverse faults that dip to the southeast (Figure 2). Ediacaran, Cambrian, and Ordovician strata are exposed in the area around the deposit. The Jianyan deposit is hosted by thick, light grey to purple, micritic silty dolostone of the Cambrian Houba Formation and by micritic bioclastic limestone and dolostone of the Ordovician Tongzi Formation (Figure 3). The vein mineralisation is stratiform or infills NE-SW-trending fractures in the host dolostone and limestone (Figure 4a). The three ore bodies are 210–500 m long, 10–30 m thick, and have ore grades of 0.2–0.3 wt.% Hg (500–2000 t Hg). The mineralisation is characterised by simple mineral assemblages that include cinnabar and minor pyrite, stibnite, and limonite. The gangue minerals are mainly calcite (50 vol.%), dolomite (40 vol.%), and quartz (10 vol.%). Cinnabar crystals are dark red (Figure 4b–4d) and occur as isolated fine to coarse grains or in polycrystalline aggregates (Figure 4e, 4f). In the Cambrian dolostone, calcite-cinnabar veins are closely associated with organic matter (Figure 4g).

4. Sampling and analytical methods

Samples with a complex mineral paragenesis were collected from ore bodies hosted in dolostone of the Cambrian Houba Formation. These samples were cut into smaller pieces to expose fresh surfaces and then attached to epoxy mounts. The mounts were carefully polished using 1000 grade emery paper before washing with Milli-Q water in an ultrasonic bath for 15 min.

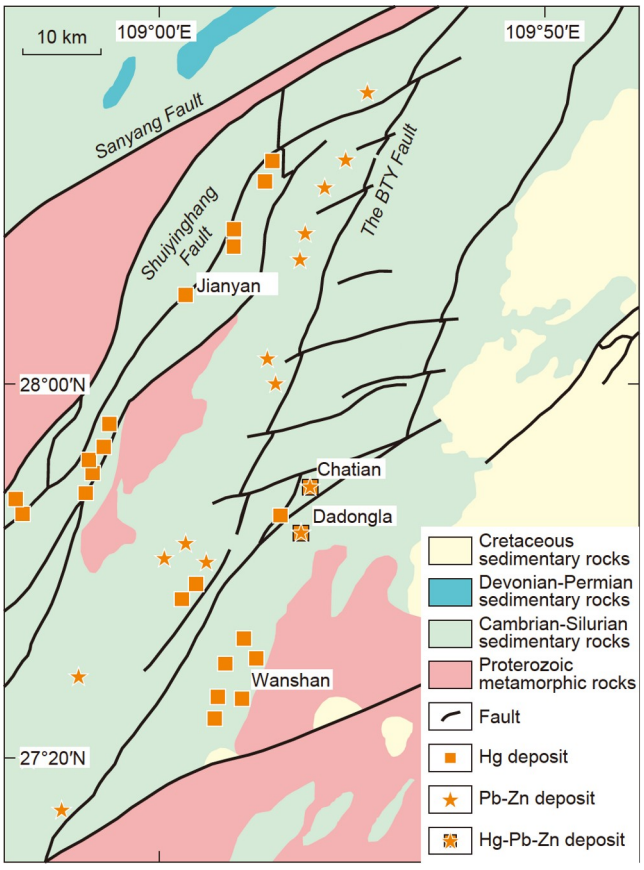

Figure 2 Simplified geological map of the Baojing-Tongren-Yuping (BTY) fault zone showing the distribution of the main Hg and Pb-Zn deposits.

Electron probe micro-analyses (EPMA) were carried out using a JEOL JXA-iSP100 at the Laboratory of Marine Element and Isotope Facilities in the Southern Marine Science and Engineering Guangdong Laboratory, Zhuhai. Major and minor elements were measured with an accelerating voltage of 15 kV, probe current of 5 nA, and beam diameter of 5 μm. The peak counting time was 10 s for major elements (Ca, Mg, Mn) and 20 s for minor elements (Ba, Sr, Fe, Si). Calcium concentrations were used as an internal calibration for analyses by laser ablation-inductively coupled plasma mass spectrometry (LA-ICP-MS).

Trace elements were determined *in situ* by LA-ICP-MS. An ASI RESOlution 193 nm excimer UV ArF LA system was employed with a dual-volume Laurin Technic ablation cell coupled to a Thermo iCap RQ quadruple ICP-MS instrument at the Radiogenic Isotope Facility (RIF), University of Queensland (UQ), Brisbane, Australia. Prior to analysis, the mounts were thoroughly cleaned with soap before being rinsed using MilliQ water in a sonic bath and then dried overnight at 60°C on a hot plate. The samples were then mounted in a sample holder and placed in the ablation cell. The mass spectrometer was tuned by scanning a NIST612 glass reference material using laser parameters of 50 μm spot

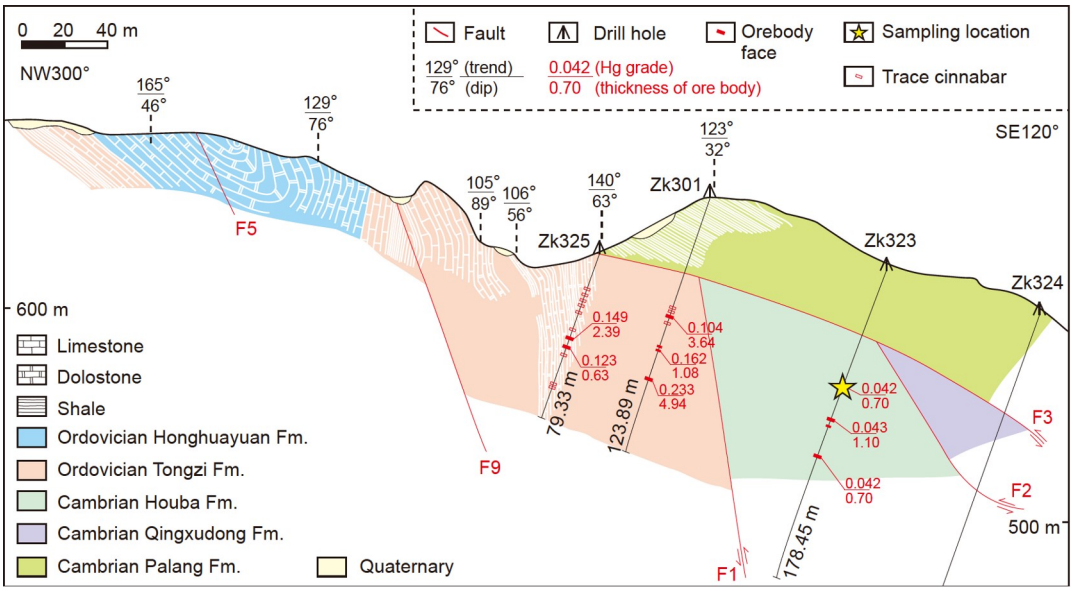

Figure 3 Cross-section through the Jianyan Hg deposit showing the location of the main mineralised structures, generally stratabound. The F3 fault plane is the major observed fault and the Cambrian shale in the hanging wall of this fault may have been a barrier to the migration of ore-forming fluids.

size, 3 μm s^{-1} speed, and 10 Hz repetition rate to optimize the sensitivity and minimize the double charge and oxidation rate. Sample ablation was undertaken using a laser beam energy density of 3 J cm^{-2}, a spot size of 100 μm, and a repetition rate of 10 Hz. The ablated aerosols were driven into a funnel before being carried to the mass spectrometer in a mixture of ultrapure He and Ar gases with a minor amount of N_2 used to boost transport efficiency and elemental intensity. The Durango and NIST-614 glass standard was employed for instrument tuning and quality control (Kendrick et al., 2020). The glass standard NIST-612 served as a reference for calculating elemental concentrations using the Iolite 3.6 software package (Paton et al., 2010). The CaO content (wt.%) was obtained using EPMA.

Five powder samples were obtained from carbonate clumps and veins in the mounted sample by micro-drilling and were used for acid-dissolution Sr isotopic analyses. Strontium isotope ratios were determined at RIF-UQ, Brisbane, Australia. Around 50 mg of calcite powder was weighed into Teflon beakers and digested in weak acetic acid to extract Sr from the carbonate fraction to avoid the leaching of any radiogenic ^{87}Sr and Rb from the non-carbonate constituents. The supernatant was separated and Sr separation was undertaken following standard cation exchange column procedures. The Sr solution was collected and measured on a Nu Plasma I multi-collector ICP-MS (MC-ICP-MS). The SRM 987 standard was measured after every 5 unknowns throughout the run and used for external calibration. Procedural Sr blanks were also included and were in general <50 pg, at least four orders of magnitude lower than the concentrations of Sr in the unknowns (>1000 ng). Long-term repeated analyses of the SRM 987 standard on this instrument yielded a mean $^{87}Sr/^{86}Sr$ value of 0.710250±0.000032 (2σ).

In situ U-Pb isotopic analyses were undertaken at the RIF-UQ, Brisbane, Australia, employing a Nu Plasma II MC-ICP-MS instrument coupled to a RESolution 193nm excimer UV ArF LA system with a dual-volume Laurin Technic ablation cell. Prior to U-Pb dating, calcite was screened and subjected to laser ablation for ~5 s per spot, with U/Pb data acquired using a Thermo iCap RQ ICP-MS. This approach removes any surficial contamination during the first 3 s of laser time and enables the identification of broad U/Pb domains (based on data acquired during the last 2 s of ablation). Calcite in the Jianyan Hg deposit has low U and Pb contents (generally <1 ppm, 1 ppm=1 μg g^{-1}), which makes it difficult to measure these elements precisely by conventional quadrupole ICP-MS or MC-ICP-MS (Kylander-Clark, 2020). As such, the highest-mass end of the collector array of the Nu Plasma II MC-ICP-MS used an electron multiplier for the measurement of ^{238}U. This discrete dynode multiplier has a sensitivity (100 μm; 3 J cm^{-2}; 10 Hz; ^{238}U>500,000 cps ppm^{-1}; ^{207}Pb blank=10–30 cps) that is 3–10 times higher than that achievable using a standard quadrupole ICP-MS instrument (Luo et al., 2020). The NIST614 glass and matrix-matched calcite standards were also analysed using standard-sample bracketing throughout the analytical period, with the resulting data used for external standardization to monitor instrumental drift in isotope measurements and laser-induced elemental fractionation. Data reduction was undertaken using the Iolite 3.6 software package (Paton et al., 2010). Approximate U and Pb concentrations for each spot were then determined using the total U and Pb isotopic counts, respectively.

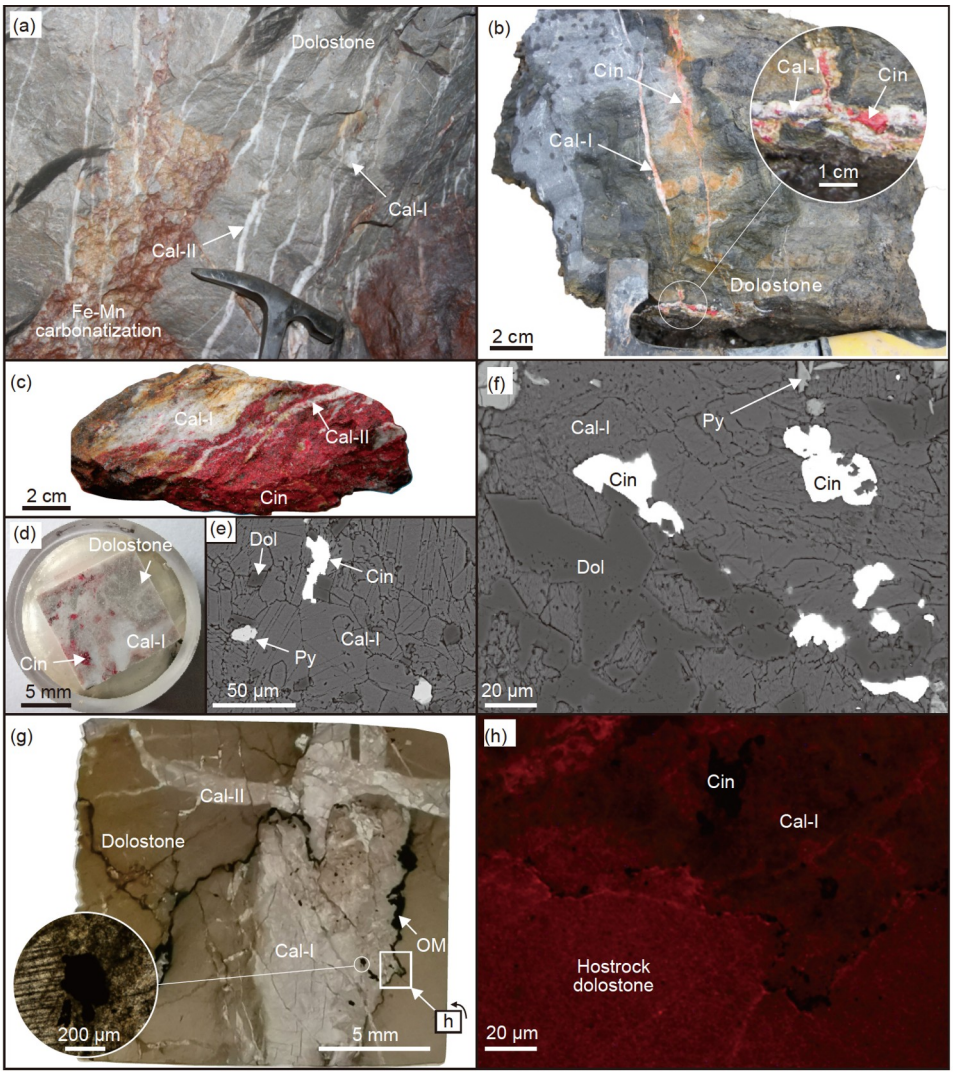

Figure 4 Photographs of the adit and hand specimen samples from the Jianyan Hg deposit. (a) Millimetre-sized calcite veinlets cutting Fe-Mn carbonates and unaltered dolostone. (b)–(d) Hand specimens showing the association between calcite and cinnabar. (e), (f) Back-scattered electron (BSE) images showing the sulphides and carbonates formed during stage I, and the relationships between calcite, dolomite (Dol), cinnabar (Cin), and pyrite (Py). (g) Photomicrograph (transmitted light) showing calcite of both stages. The white rectangle indicates the area that was imaged under CL. OM, Organic Matter. (h) CL image of host dolostone and Cal-I.

Mass-bias correction of the $^{238}U/^{206}Pb$ data was undertaken using the 3.001±0.012 Ma (2σ) calcite speleothem ASH-15D standard that was previously dated by thermal ionization mass spectrometry (TIMS; Mason et al., 2013; Vaks et al., 2013; Nuriel et al., 2017) and the 209.8±1.3 Ma (weighted mean age; n=21, MSWD=2.7) AHX-1a standard that was previously dated by LA-MC-ICP-MS (Cheng et al., 2020). The corrected U-Pb isotopic data for the calcite AHX-1a standard were plotted on a $^{238}U/^{206}Pb$ vs. $^{207}Pb/^{206}Pb$ Tera-Wasserburg diagram using IsoplotR (Vermeesch, 2018) to obtain the measured age. The offset factor between the measured age and the true age of this calcite standard was used to normalize the $^{238}U/^{206}Pb$ ratios of unknowns using the approach of Roberts et al. (2017). Following normalization, the U-Pb isotopic data for unknowns were plotted on Tera-Wasserburg diagrams. We further verified the reliability of the ages by comparison with LA-ICP-MS U-Pb analyses of different samples from the same vein. The methods are presented in Appendix 2.

5. Results

5.1 Calcite mineralogy

Calcite from the Jianyan Hg deposit grew during two stages: syn-ore Cal-I and post-ore/barren Cal-II. Cal-I occurs in veins and is associated with cinnabar, Fe-Mn carbonate alteration (Figure 4a), and limonite. Cal-II is observed mainly in narrow, white, network-like veins that cut the host dolostone and Cal-I.

The Cal-I veins typically occur as milky white clusters (<10 cm) that are associated with local Fe-Mn carbonate

alteration in the dolostone host and organic matter (Figure 4g). The Cal-I crystals are generally euhedral-subhedral and relatively small (<100 μm), and have a rhombic cleavage (Figure 4g). Under cathodoluminescence (CL) imaging, Cal-I crystals are dark-orange in colour. The host dolostone typically shows brighter luminescence with red-orange colours (Figure 4h). In most cases, Cal-I and adjacent cinnabar share the same flat crystal face and are locally coupled to form intergrown structures, indicating they grew together. Cubic pyrite only occurs within Cal-I crystals (Figure 4e, 4f).

The barren stage is represented by Cal-II, with no significant presence of dolomite, ore minerals, or organic matter. Cal-II occurs as narrow, white network-type veins that crosscut host dolostone and Cal-I (Figure 4a). Cal-II is typically subhedral-anhedral, coarser (>100 μm) than Cal-I, and displays dark-grey colour in CL images (Appendix 2).

5.2 *In situ* trace element data

The LA-ICP-MS trace element data for calcite from the Jianyan Hg deposit are presented in Appendix 1. Both Cal-I and Cal-II have uniform Fe contents of 95.4–103 ppm (mean 98.2 ppm; n=46) and 95.0–103 ppm (mean 97.5 ppm; n=20), respectively. However, they have relatively variable Mn contents of 16.9–32.9 ppm (mean 27.4 ppm; n=46) and 37.4–64.2 ppm (mean 52.0 ppm; n=20), respectively. The host dolostone has higher Fe (155–6989 ppm; mean 1125 ppm; n=19) and Mn (45.1–64.8 ppm; mean 53.3 ppm; n=19) contents than the calcite (Figure 5a). Cal-I and Cal-II have total rare earth element contents (ΣREE= 2.48–55.8 ppm; mean 17.5 ppm) and Eu anomalies (δEu=0.6–1.0; mean 0.7) similar to those of the host dolostone. The host dolostone and Cal-I have similar La/Y ratios (0.8–4.4; mean 1.9; n=65), different from Cal-II (0.3–1.7; mean 0.7; n=20) (Figure 5b). The host dolostone, Cal-I, and Cal-II have slightly different chondrite-normalised REE patterns (Figure 6a–6c), and yield light REE/heavy REE ratios of 12.7–15.7 (mean 14.2), 11.4–47.8 (mean 22.5), and 5.9–16.1 (mean 8.7), respectively. Cal-I has slightly higher U/Pb ratios and a wider range of values than Cal-II. Cal-I and Cal-II have U/Pb ratios of 1.1–17.8 (mean 3.9; n=40) and 0.1–1.2 (mean 0.6; n=84), respectively.

5.3 Strontium isotope ratios

$^{87}Sr/^{86}Sr$ ratios of calcite from the Jianyan deposit range from 0.710227 to 0.710907 (2σ; Appendix 1). Cal-I yields $^{87}Sr/^{86}Sr$=0.710381–0.710907 (n=3), similar to Cal-II (0.710227–0.710440; n=4) (Figure 7).

5.4 *In situ* calcite U-Pb ages

Cal-I associated with cinnabar from the Jianyan deposit has

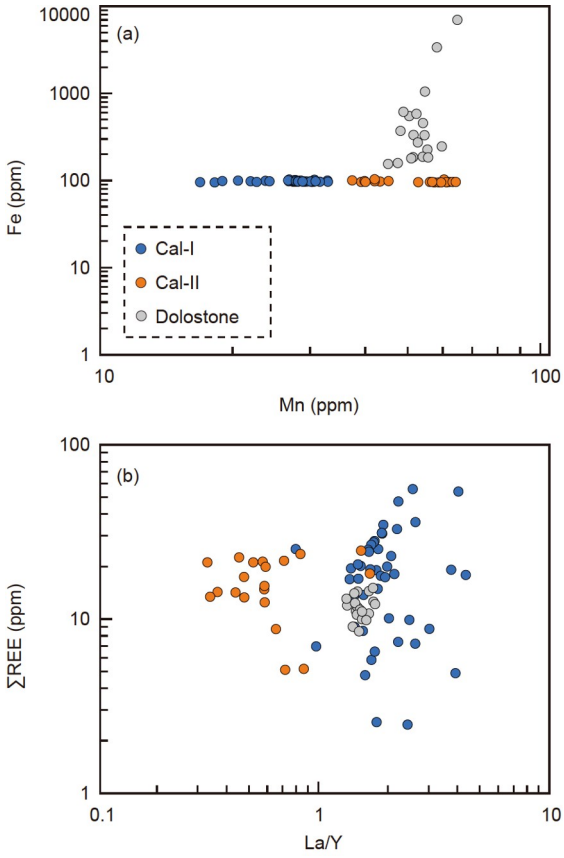

Figure 5 Compositional variations (LA-ICP-MS) of carbonate minerals from different stages in the Jianyan Hg deposit. (a) Fe versus Mn diagram. Cal-I and Cal-II have similar Fe contents, but Cal-II has higher Mn contents. The dolostone host rock has higher Fe-Mn contents. (b) REE versus La/Y diagram. Cal-I and the host rocks have similar REE contents, higher than those of Cal-II, which have lower La/Y ratios.

$^{238}U/^{206}Pb$ ratios of 1.7–4.2, making it suitable for dating. Cal-I has U and Pb concentrations of 0.101–1.348 ppm (mean 0.420 ppm) and 0.024–0.783 ppm (mean 0.276 ppm), respectively (Figure 8a, 8b; Appendix 1). Twenty-eight analyses yielded a well-defined isochron with an age of 426.3±5.7 Ma (MSWD=1.5), with low uncertainties (i.e., <1%; 2σ) on the U and Pb isotope ratios and a good signal intensity. Analysis of the matrix-matched carbonate ASH-15D standard (3.001±0.012 Ma; Mason et al., 2013; Vaks et al., 2013; Nuriel et al., 2017) yielded an age that agrees well with its known age (3.10±0.18 Ma; MSWD=2.0; Appendix 2), confirming that ages obtained for unknown calcite grains are accurate.

LA-ICP-MS U-Pb analyses of different samples from the same vein yielded an age of 416.9±39.7 Ma (MSWD=2.1; Figure 8c, 8d). This age has a large uncertainty because of the low U/Pb ratios, but is within uncertainty of the first age obtained by LA-MC-ICP-MS. Therefore, the 426.3±5.7 Ma age obtained for the syn-ore calcite in the Jianyan Hg deposit is inferred to be geologically meaningful and constrains the timing of Hg mineralisation in the study area.

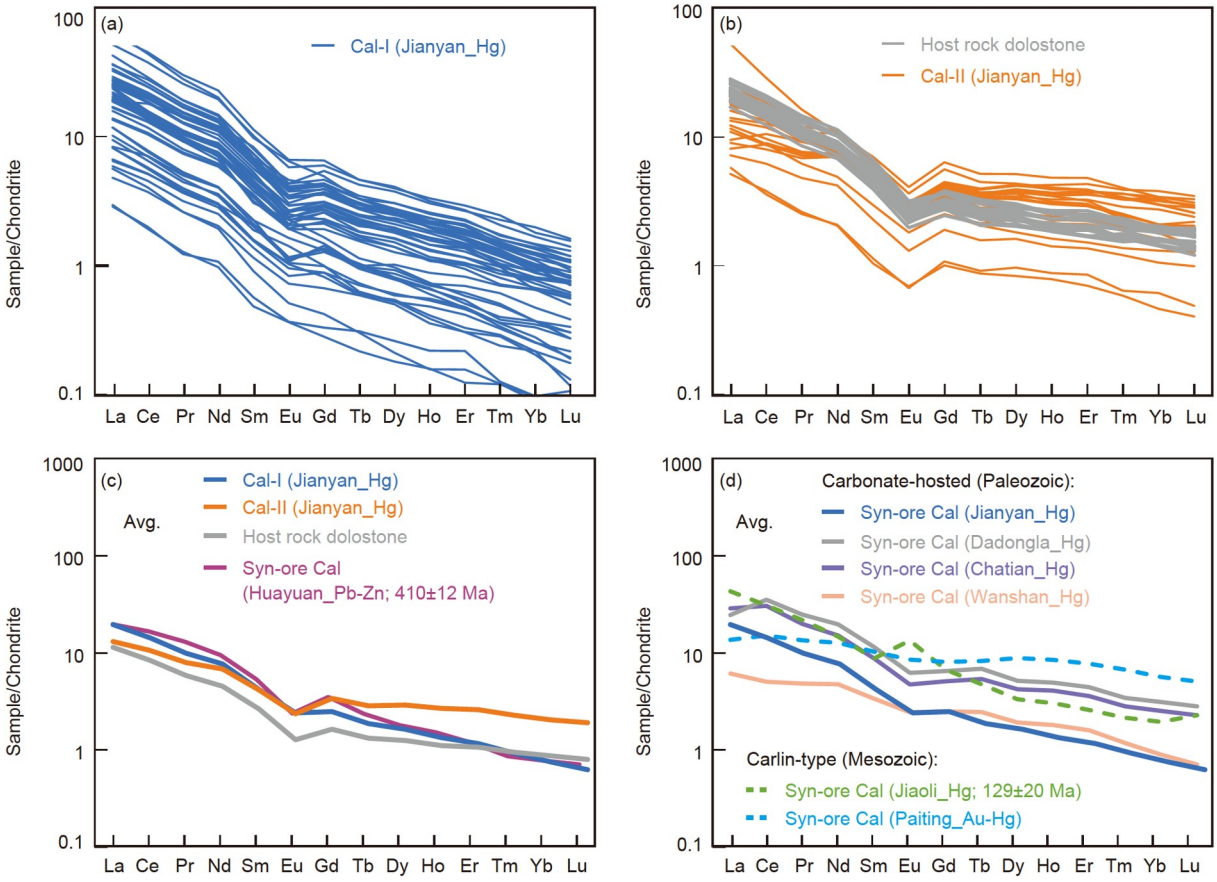

Figure 6 Chondrite-normalised REE patterns for (a) Cal-I and Cal-II and (b) the host dolostone in the Jianyan Hg deposit. (c) Comparison of chondrite-normalised REE patterns for carbonates from the Jianyan Hg deposit with the average composition of syn-ore calcite from the adjacent Huayuan Pb-Zn deposit (Wei et al., 2017). (d) Chondrite-normalised REE patterns for syn-ore calcite in Hg deposits in the South China low-temperature mineralisation domain (Wang et al., 2010; Han et al., 2017; Li et al., 2020). All data are normalised to the chondritic composition of Sun and McDonough (1989). Avg represents the average contents. The ages of mineral deposits are from Duan et al. (2014) and Wang and Wen (2015).

6. Discussion

6.1 Differentiation of calcite of the syn-ore and barren stages from the Jianyan Hg deposit

In the field, it is difficult to distinguish calcite that formed during the syn-ore and barren stages in terms of texture and colour, especially given the local occurrence of cinnabar in the veins. However, the trace element and isotopic compositions of calcite may contain information about the ore-forming fluids and can be used to constrain its origin (Fusswinkel et al., 2013; Smith-Schmitz and Appold, 2018). The two stages of hydrothermal calcite identified in the Jianyan Hg deposit have similar Fe but variable Mn contents (Figure 5a). Given that Mn^{2+} is the dominant luminescence activator (Peyrotty et al., 2020), host dolostone with higher Mn contents has lighter CL compared with hydrothermal calcite. Although Fe is the main CL quencher in carbonates, relatively low Fe contents may have little effect on the CL images of the Jianyan carbonates (cf. Marshall, 1988). The low Fe/Mn ratios (1.5–2.7) of Cal-II might cause a darker CL compared with host dolostone and Cal-I.

Syn-ore Cal-I exhibits highly variable La/Y and ΣREE values, which contrast with the more uniform compositions of the host dolostone (Figure 5b). The compositions of Cal-I and Cal-II contrast with those of the host dolostone, suggesting that syn-ore Cal-I was not derived from these host rocks by dissolution and re-precipitation, but instead was derived from a deep-seated source. Cal-I has higher La/Y and light REE/heavy REE ratios than Cal-II, suggesting different origins of the hydrothermal fluids of the syn-ore and barren stages (Luo et al., 2020). Cal-I can be further chemically distinguished from barren Cal-II by U/Pb ratios, with Cal-I having relatively high U/Pb ratios.

6.2 Geochemistry of calcite in ore deposits of South China

The variable light REE/heavy REE ratios of calcite from the Jianyan deposit might be due to compositionally variable fluids with different REE contents and originating from different type of rocks (Michard and Albarède, 1986). The abundance of hydrothermal fluorite in the mineralisation belt

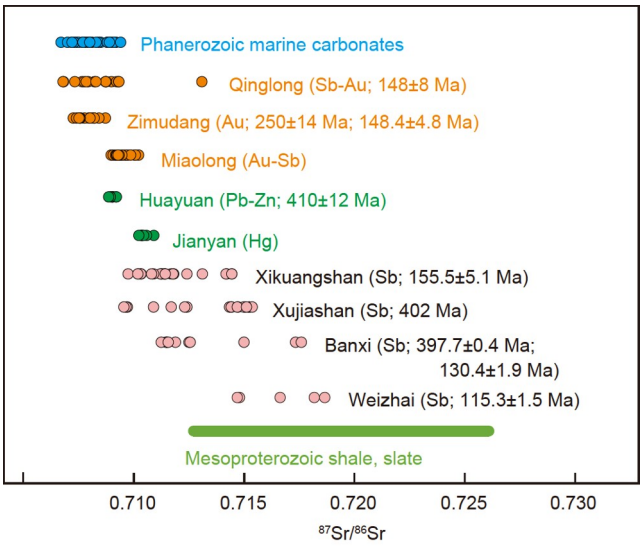

Figure 7 $^{87}Sr/^{86}Sr$ values for the hydrothermal Au, Hg, Sb, and Pb-Zn deposits, Mesoproterozoic rocks in South China (Peng et al., 2003b), and Phanerozoic marine carbonates (Veizer and Compston, 1974). The $^{87}Sr/^{86}Sr$ values of the mineral deposits and references are listed in Appendix 1. The ages of the mineral deposits are from Peng et al. (2003b), Wang et al. (2012), Wang (2013), Duan et al. (2014), Li H et al. (2018), and Luo et al. (2020).

indicates that the REEs are unlikely to have been mobilised by fluoro-complexes, due to the strong affinity of Ca^{2+} for F^{-}, which would have buffered the concentration of ligands available for complexation in solution (Bau and Dulski, 1995; Salvi and Williams-Jones, 1996). Consequently, the REEs were likely mobilised by Cl complexation, given the higher stability of Cl complexes compared with other mobilising ligands in hydrothermal Hg-Pb-Zn mineralising systems (Barnes, 1997). This contrasts with the preferential mobilisation of heavy REEs in near-neutral to slightly alkaline fluids rich in (bi)carbonate ligands in Mesozoic hydrothermal Au-Sb mineralising systems of South China (Wang et al., 2010; Tan et al., 2017). The REE patterns of calcite from the Jianyan deposit are similar to those of calcite in the carbonate-hosted Dadongla, Chatian, and Wanshan Hg ±(Pb±Zn) deposits (Wang et al., 2010) and in the Caledonian Huayuan Pb-Zn ore field (Wei et al., 2017), but differ markedly from those of calcite from the Mesozoic Jiaoli Hg (Han et al., 2017) and Paiting Hg-Au (Xie et al., 2017) deposits (Figure 6d).

Calcite crystals from carbonate-hosted Hg-Pb-Zn-Ba-F deposits in the WHEG mineralisation belt have a narrow range of negative Eu anomalies (δEu=0.5–1.0; Figure 6d), which contrasts with the positive Eu anomalies (δEu>1.0) of calcite in Mesozoic ore deposits in South China (Wang et al., 2010). Thermodynamic calculations and theoretical considerations suggest that temperature is the main control on

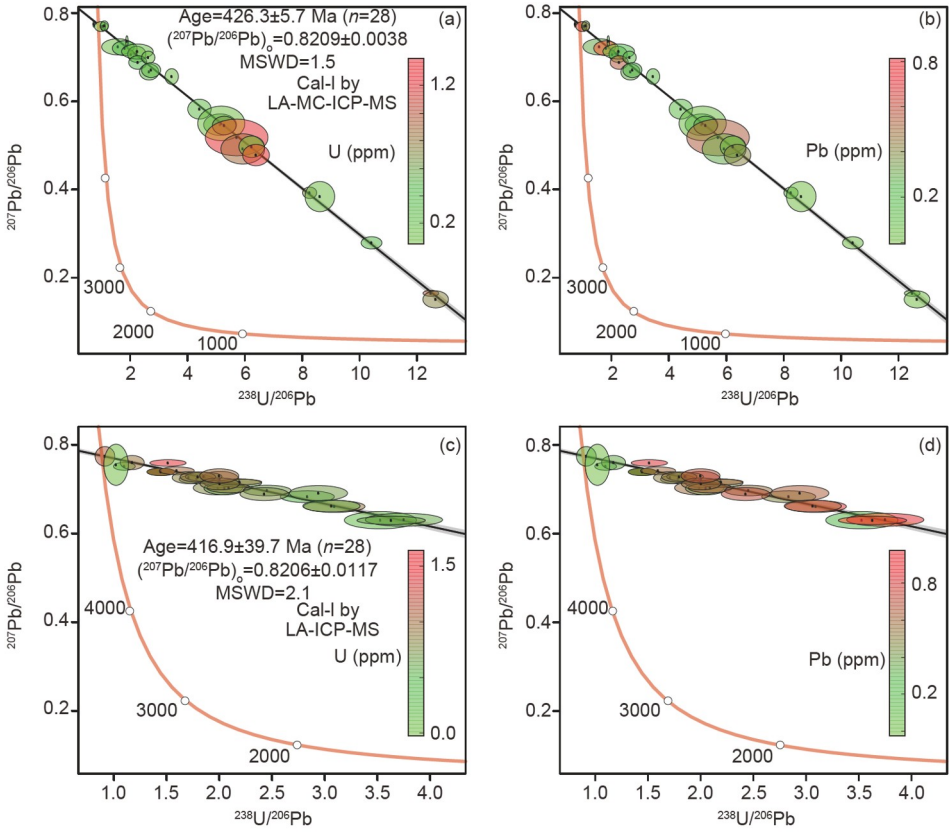

Figure 8 Tera-Wasserburg concordia diagrams for syn-ore calcite in the Jianyan Hg deposit, analysed by LA-MC-ICP-MS ((a), (b)) and LA-ICP-MS ((c), (d)). The U and Pb contents represented by red to green shading are in parts per million. Error ellipses indicate the 2σ uncertainty.

the Eu^{3+}/Eu^{2+} ratio of hydrothermal systems (Bau and Moller, 1992). For temperatures of >200°C, Eu^{2+} dominates over Eu^{3+}, with the former preferentially substituting for Ca^{2+} as compared with trivalent REEs. Hydrothermal fluids that precipitate under such conditions would form minerals with positive Eu anomalies. Therefore, the carbonate-hosted Hg-Pb-Zn-Ba-F deposits might have formed at relatively low temperatures of <200°C, which is consistent with the low homogenisation temperatures (90–170°C) of fluid inclusions in calcite from the mineralisation belt (Wang et al., 2010).

The Sr isotope ratios ($^{87}Sr/^{86}Sr$=0.710381–0.710907) of syn-ore calcite in the Jianyan Hg deposit are relatively uniform, and contrast with the highly variable Sr isotope ratios (0.712700–0.726100) of Proterozoic basement rocks in the study area (Figure 7; Peng and Hu, 2001; Xiao, 2014; Sun et al., 2016; Li H et al., 2018). This indicates that metals in the Jianyan deposit were not derived from the Proterozoic basement rocks, which contrasts with the source of metals in the Sb deposits (Chen et al., 2020).

In general, the high La/Y ratios (>~1.0), negative Eu anomalies (δEu=0.5–1.0), and moderate and relatively homogeneous $^{87}Sr/^{86}Sr$ ratios (0.710381–0.710907) of syn-ore calcite in the Jianyan deposit are similar to other carbonate-hosted Hg-Pb-Zn-Ba-F deposits in the region, but are distinct from Mesozoic ore deposits in South China.

6.3 Interpretation of age data and implications

In South China, Hg deposits occur in two mineralisation belts, as inferred from the different metal associations and spatial distributions: (1) the WHEG carbonate-hosted Hg-Pb-Zn-Ba-F mineralisation belt; and (2) the Youjiang Basin Carlin-type Hg-Au-As-Sb mineralisation belt (Su et al., 2009; Zhou Y et al., 2015). However, it is unclear whether the two belts were formed during the same event. Previous studies have focused mainly on the Carlin-type Hg-rich deposits that are related to Mesozoic extension or directly associated with normal faults (Hu et al., 2002, 2017; Mao et al., 2013). For the WHEG carbonate-hosted Hg-Pb-Zn-Ba-F belt, the timing of mineralisation is still controversial, despite the numerous dating methods that have been used, such as calcite/fluorite Sm-Nd, quartz fluid inclusion Rb-Sr, and sphalerite Rb-Sr dating. Samples from the Hg-Pb-Zn-Ba-F mineralisation belt have yielded variable ages of 470–377 Ma (Figure 9; e.g., Duan et al., 2014; Wang and Wen, 2015).

The Hg deposits along the south-eastern margin of the Yangtze Block are spatially associated with Pb-Zn and Ba-F deposits. These deposits exhibit vertical zoning, with the Ba-F deposits being hosted mainly in the Early Ordovician carbonate rocks, and the Hg and Pb-Zn deposits in the middle to late Cambrian carbonate rocks (Zhang et al., 2018; Fu, 2019). The barite, fluorite, and other gangue minerals are commonly associated with or occur adjacent to Pb-Zn ore bodies (e.g., the Qianchanggai Pb-Zn deposit and the Weijiazhuang and Guihua fluorite deposits) (Zou et al., 2022). Cinnabar is also commonly associated with sphalerite. The Hg and Pb-Zn ore bodies are lenticular, have a similar strike, and are controlled by the same faults and folds. Some Pb-Zn deposits, including the Chatian and Dadongla deposits, show lateral zoning from Hg to Zn from the centre to the periphery of ore bodies or from near to far from fractures. In the transition zone, mixed ores of cinnabar and sphalerite are observed (Yang et al., 2014; Fu et al., 2017).

Given the high solubility of halogen complexes, such as $BaCl_2$, $(HgCl_2)^0$, $(HgCl)^+$, $(HgCl_3)^-$, $(HgCl_4)^{2-}$, $(PbCl_4)^{2-}$, and $(ZnCl_4)^{2-}$, large-scale F- and Cl-rich brines might have been important in the base metal and Ba mineralization (Barnes, 1997; Banks et al., 2002; Smith-Schmitz and Appold, 2021). In contrast, Au chloride complexes (predominantly $AuCl^{2-}$) are soluble in high-temperature fluids (>300°C) with a low pH and elevated salinity, whereas aqueous S complexes of Au are dominant in medium-temperature fluids (<300°C) that are weakly acidic and have elevated levels of dissolved S. Hence, the nature of the ore-forming fluids in the carbonate-hosted, low-temperature Hg-Pb-Zn-Ba-F deposits was likely different from that of the Mesozoic Carlin-type deposits.

In this study, a calcite U-Pb age of 426.3±5.7 Ma was obtained for the Jianyan Hg deposit, which is within uncertainty of the ages of the Huayuan Pb-Zn (410±12 Ma; sphalerite Rb-Sr) and Dazhuyuan Ba-F (430±13 Ma; calcite Sm-Nd) deposits (Duan et al., 2014; Zhang et al., 2018), and comparable to the ages of the Jiangjiaya (372.0±9.8 Ma) and Tangbian (477±5 Ma) Pb-Zn deposits (Zhou Y et al., 2015; Yu et al., 2017). Calcite geochemical data further suggest a similar genesis for the Jianyan Hg and Huayuan Pb-Zn deposits (Figures 6 and 7). The *ca*. 426 Ma mineralisation event may have been related to tectonothermal events during the Late Caledonian Orogeny (Chu et al., 2012). The Jiangnan Orogenic Belt in South China underwent extensive early Paleozoic granitic magmatism that formed a series of gneissic and massive granite intrusions (Shu, 2006). These granites have zircon U-Pb ages of 480–398 Ma, with a peak at 456–419 Ma that is indicative of a transition between an intracontinental orogeny and subsequent crustal extension (Figure 10a; Faure et al., 2009; Charvet et al., 2010). Movement on NE-SW-trending Caledonian reverse faults caused the inversion of a range of units from the Neoproterozoic Banxi Group to the Early Ordovician sedimentary rocks. Local extensional tectonism during the early Paleozoic orogeny was favourable for the migration of basinal brines along the margins of the Jiangnan Orogenic Belt, forming Hg, Pb-Zn, and Ba-F ore bodies (Figure 10b). These Caledonian ore bodies are carbonate-hosted and related to low-temperature polymetallic fluids that differ from the

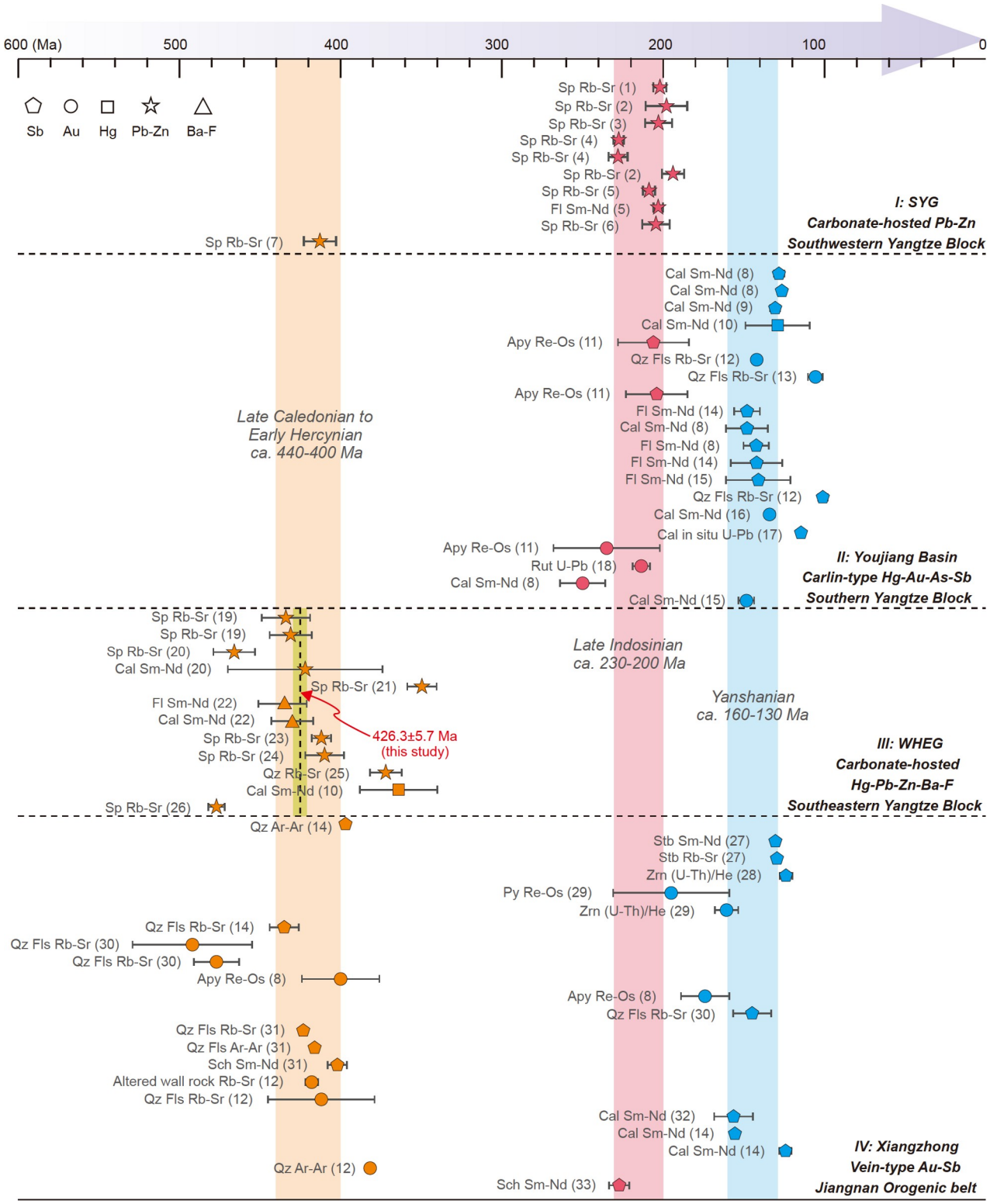

Figure 9 Compiled ages for low-temperature mineralisation systems in South China, including the Jianyan deposit (this study). Data sources: 1, Lin et al. (2010); 2, Zhou et al. (2013); 3, Zhang et al. (2014); 4, Han et al. (2007); 5, Zhou J X et al. (2015); 6, Yang et al. (2019); 7, Xiong et al. (2018); 8, Wang (2012); 9, Xiao (2014); 10, Wang and Wen (2015); 11, Chen et al. (2015); 12, Hu et al. (2007); 13, Su et al. (1998); 14, Peng et al. (2003b); 15, Wang (2013); 16, Su et al. (2009); 17, Luo et al. (2020); 18, Pi et al. (2017); 19, Cao et al. (2015); 20, Yang et al. (2016); 21, Liao et al. (2015); 22, Zhang et al. (2018); 23, Tan et al. (2018); 24, Duan et al. (2014); 25, Zhou Y et al. (2015); 26, Yu et al. (2017); 27, Li H et al. (2018); 28, Li et al. (2020); 29, Fu et al. (2019); 30, Zhang et al. (2020); 31, Peng et al. (2003a); 32, Hu et al. (1996); 33, Wang et al. (2012). Abbreviations: Sp, sphalerite; Fl, fluorite; Cal, calcite; Apy, arsenopyrite; Qz, quartz; Py, pyrite; Stb, stibnite; Zrn, zircon; Rut, rutile; Sch, scheelite.

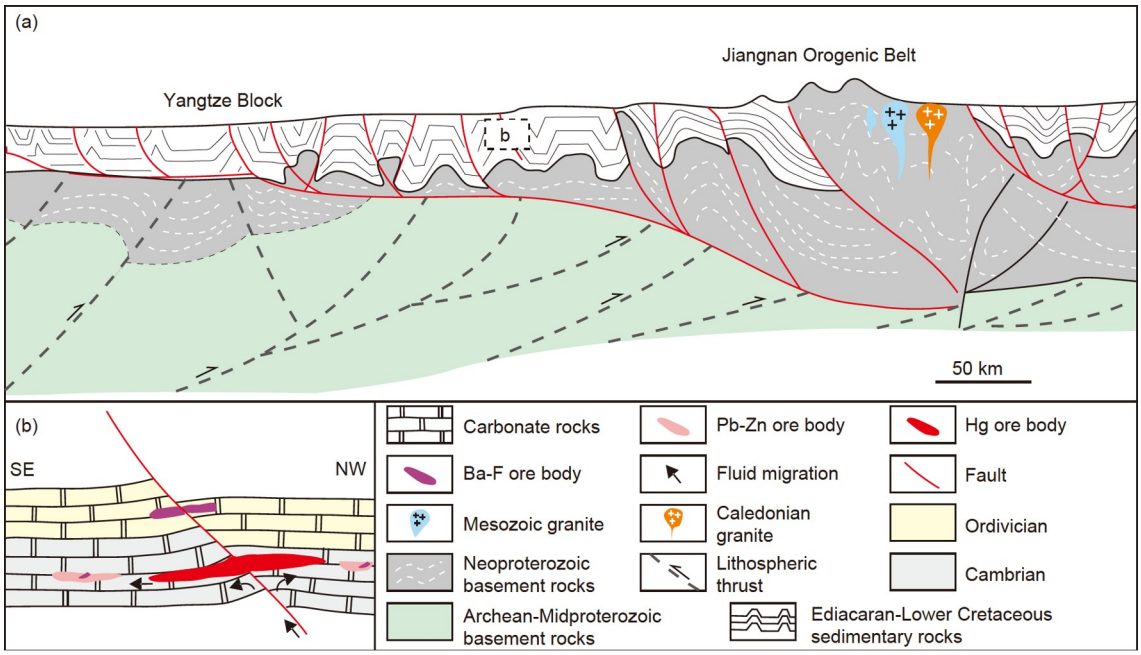

Figure 10 Simplified geodynamic model of the WHEG carbonate-hosted Hg-Pb-Zn-Ba-F mineralisation belt during the early Paleozoic intracontinental orogeny, showing the migration of brine enriched in metals and precipitating ores within the carbonate rocks, commonly close to faults. (a) Sketch representing the tectonic setting at ca. 425 Ma, of the WHEG carbonate-hosted Hg-Pb-Zn-Ba-F mineralisation belt. The cross-section is modified from the seismic profile of Li et al. (2019). (b) Simplified sketch representing the circulation of hydrothermal Hg-rich fluids in fault and in lithological contact, showing the zoning of ore-forming elements during their precipitation.

classical Mesozoic polymetallic mineralisation of South China.

7. Conclusions

(1) Syn-ore calcite from the Jianyan Hg deposit can be distinguished from calcite in Mesozoic Hg deposits in South China by its high La/Y ratios, negative Eu anomalies, and uniform $^{87}Sr/^{86}Sr$ ratios.

(2) The syn-ore Cal-I yields a U-Pb age of *ca*. 426 Ma that constrains the timing of Hg mineralisation to the middle Silurian. This mineralisation event was associated with the early Paleozoic Caledonian orogeny and is distinct from the common Mesozoic polymetallic mineralisation in South China.

(3) The mineral chemistry and U-Pb dating of calcite have the potential to distinguish different mineralisation events in low-temperature ore systems.

Acknowledgements *We thank the Non-Ferrous Metals and Nuclear Industry Geological Exploration Bureau of Guizhou for assistance during fieldwork; Ai Duc NGUYEN, Gang XIA (The University of Queensland, Brisbane) for help in the laboratory; and Yong-Bin WANG (Yunnan University, Kunming) and Zhi-Long HUANG, Zhen-Zhong XIANG, and Zhuo-Jun XIE (Institute of Geochemistry, Chinese Academy of Sciences, Guiyang) for fruitful discussions. This research was financially supported by the National Natural Science Foundation of China (Grant Nos. 41872095, U1812402, and 42172082), the Research Startup Project of Yunnan University (Grant No. YJRC4201804), and the Talents Program Project of Yunnan Province (Grant No. YNQR-QNRC-2018-104) to Jiaxi ZHOU.*

References

Banks D A, Boyce A J, Samson I M. 2002. Constraints on the origins of fluids forming Irish Zn-Pb-Ba deposits: Evidence from the composition of fluid inclusions. Econ Geol, 97: 471–480

Barnes H L. ed. 1997. Geochemistry of Hydrothermal Ore Deposits. Hoboken: John Wiley & Sons

Bau M, Dulski P. 1995. Comparative study of yttrium and rare-earth element behaviours in fluorine-rich hydrothermal fluids. Contrib Mineral Petrol, 119: 213–223

Bau M, Moller P. 1992. Rare earth element fractionation in metamorphogenic hydrothermal calcite, magnesite and siderite. Mineral Petrol, 45: 231–246

Bradley D C, Leach D L. 2003. Tectonic controls of Mississippi Valley-type lead-zinc mineralization in orogenic forelands. Miner Depos, 38: 652–667

Cao L, Duan Q F, Zhou Y. 2015. Rb-Sr dating of sphalerites from the Aozigang zinc deposit in Hubei Province and its geological significance (in Chinese). Geol China, 42: 235–247

Charvet J, Shu L, Faure M, Choulet F, Wang B, Lu H, Breton N L. 2010. Structural development of the Lower Paleozoic belt of South China: Genesis of an intracontinental orogen. J Asian Earth Sci, 39: 309–330

Chen J F, Foland K A, Xing F M, Xu X, Zhou T X. 1991. Magmatism along the southeast margin of the Yangtze block: Precambrian collision of the Yangtze and Cathysia blocks of China. Geology, 19: 815

Chen J, Yang R D, Du L J, Gao J B, Zheng L L, Huang Z L. 2020. Multistage fluid sources and evolution of Qinglong Sb-(Au) deposit in northern margin of Youjiang basin, SW China: REE geochemistry and Sr-H-O isotopes of ore-related jasperoid, quartz and fluorite. Ore Geol Rev, 127: 103851

Chen M H, Mao J W, Li C, Zhang Z Q, Dang Y. 2015. Re-Os isochron ages for arsenopyrite from Carlin-like gold deposits in the Yunnan-Guizhou-

Guangxi “golden triangle”, southwestern China. Ore Geol Rev, 64: 316–327
Cheng T, Zhao J X, Feng Y X, Pan W Q, Liu D Y. 2020. *In-situ* LA-MC-ICPMS U-Pb dating method for low-uranium carbonate minerals. Chin Sci Bull, 65: 150–154
Chu Y, Lin W, Faure M, Wang Q C, Ji W B. 2012. Phanerozoic tectonothermal events of the Xuefengshan Belt, central South China: Implications from U-Pb age and Lu-Hf determinations of granites. Lithos, 150: 243–255
Cline J S, Hofstra A H, Muntean J L, Tosdal R M, Hickey K A. 2005. Carlin-type gold deposits in Nevada: Critical geologic characteristics and viable models. Economic Geology, One Hundredth Anniversary Volume. https://doi.org/10.5382/AV100
Duan Q F, Cao L, Zeng J K, Zhou Y, Tang Z Y, Li K. 2014. Rb-Sr dating of sphalerites from Shizishan Pb-Zn deposit and its geological significance in Huayuan Ore Concentration Area, Western Hunan (in Chinese). Earth Sci—J China Univ Geosci, 39: 977–999
Faure M, Shu L S, Wang B, Charvet J, Choulet F, Monie P. 2009. Intracontinental subduction: A possible mechanism for the Early Palaeozoic Orogen of SE China. Terra Nova, 21: 360–368
Fu S L, Hu R Z, Yan J, Lan Q, Gao W. 2019. The mineralization age of the Banxi Sb deposit in Xiangzhong metallogenic province in southern China. Ore Geol Rev, 112: 103033
Fu S Y, Li Z H, He C P, Zheng Z F, Tang F P, Deng L, Zhang H, Li H J. 2017. Relationship between geological structure and mineralization of mercury-lead-zinc deposit in the Fenghuang area (in Chinese). Geol Sur China, 4: 15–23
Fu S Y. 2019. Research on controlling factors of the mercury and mercury-zinc deposits in Cambrian Aoxi Formation of Fenghuang area, Hunan Province (in Chinese). Geol Sur China, 6: 42–47
Fusswinkel T, Wagner T, Wenzel T, Wälle M, Lorenz J. 2013. Evolution of unconformity-related MnFeAs vein mineralization, Sailauf (Germany): Insight from major and trace elements in oxide and carbonate minerals. Ore Geol Rev, 50: 28–51
Giorno M, Barale L, Bertok C, Frenzel M, Looser N, Guillong M, Bernasconi S M, Martire L. 2022. Sulfide-associated hydrothermal dolomite and calcite reveal a shallow burial depth for Alpine-type Zn-(Pb) deposits. Geology, 50: 853–858
Han R S, Liu C Q, Huang Z L, Chen J, Ma D Y, Lei L, Ma G S. 2007. Geological features and origin of the Huize carbonate-hosted Zn-Pb-(Ag) District, Yunnan, South China. Ore Geol Rev, 31: 360–383
Han Z C, Wang J S, Gao Z H. 2017. Geochemical characteristics and implications of REE, carbon and oxygen isotopes of calcite from la'e mercury deposit (in Chinese). J Kunming Univ Sci Technol-Nat Sci Ed, 42: 28–37
Hu R Z, Fu S L, Huang Y, Zhou M F, Fu S H, Zhao C H, Wang Y J, Bi X W, Xiao J F. 2017. The giant South China Mesozoic low-temperature metallogenic domain: Reviews and a new geodynamic model. J Asian Earth Sci, 137: 9–34
Hu R Z, Su W C, Bi X W, Tu G Z, Hofstra A H. 2002. Geology and geochemistry of Carlin-type gold deposits in China. Miner Depos, 37: 378–392
Hu R Z, Peng J T, Ma D S, Su W C, Shi C H, Bi X W, Tu G C. 2007. Epoch of large-scale low-temperature mineralizations in southwestern Yangtze massif (in Chinese). Miner Depos, 26: 583–596
Hu X W, Pei R F, Su Z. 1996. Sm-Nd dating for antimony mineralization in the Xikuangshan deposit, Hunan, China. Res Geol, 46: 227–231
Jin X Y, Zhao J X, Feng Y X, Hofstra A H, Deng X D, Zhao X F, Li J W. 2021. Calcite U-Pb dating unravels the age and hydrothermal history of the giant Shuiyindong Carlin-type gold deposit in the golden triangle, South China. Econ Geol, 116: 1253–1265
Kendrick M A, Caulfield J T, Nguyen A D, Zhao J X, Blakey I. 2020. Halogen and trace element analysis of carbonate-veins and Fe-oxy-hydroxide by LA-ICPMS: Implications for seafloor alteration, Atlantis Bank, SW Indian Ridge. Chem Geol, 547: 119668
Kylander-Clark A R C. 2020. Expanding limits of laser-ablation U-Pb calcite geochronology. Geochronology, 2: 343–354
Leach D L, Bradley D, Lewchuk M T, Symons D T, de Marsily G, Brannon J. 2001. Mississippi Valley-type lead-zinc deposits through geological time: Implications from recent age-dating research. Miner Depos, 36: 711–740
Li H, Danišík M, Zhou Z K, Jiang W C, Wu J H. 2020. Integrated U-Pb, Lu-Hf and (U-Th)/He analysis of zircon from the Banxi Sb deposit and its implications for the low-temperature mineralization in South China. Geosci Front, 11: 1323–1335
Li H, Wu Q H, Evans N J, Zhou Z K, Kong H, Xi X S, Lin Z W. 2018. Geochemistry and geochronology of the Banxi Sb deposit: Implications for fluid origin and the evolution of Sb mineralization in central-western Hunan, South China. Gondwana Res, 55: 112–134
Li S Z, Suo Y H, Li X Y, Zhou J, Santosh M, Wang P C, Wang G Z, Guo L L, Yu S Y, Lan H Y, Dai L M, Zhou Z Z, Cao X Z, Zhu J J, Liu B, Jiang S H, Wang G, Zhang G. 2019. Mesozoic tectono-magmatic response in the East Asian ocean-continent connection zone to subduction of the Paleo-Pacific Plate. Earth-Sci Rev, 192: 91–137
Li Y Q, He D F, Li D, Lu R Q, Fan C, Sun Y P, Huang H Y. 2018. Sedimentary provenance constraints on the Jurassic to Cretaceous paleogeography of Sichuan Basin, SW China. Gondwana Res, 60: 15–33
Li Z X, Li X H, Kinny P D, Wang J, Zhang S, Zhou H. 2003. Geochronology of Neoproterozoic syn-rift magmatism in the Yangtze Craton, South China and correlations with other continents: Evidence for a mantle superplume that broke up Rodinia. Precambrian Res, 122: 85–109
Liao Z W, Wang S W, Sun X M, Jiang X F, Zhou Q, Xu X Y, Guo Y. 2015. Rb-Sr dating of sphalerites from MVT Pb-Zn deposits in northeastern Guizhou Province and its geological implications (in Chinese). Miner Depos, 34: 769–785
Lin Z Y, Wang D H, Zhang C Q. 2010. Rb-Sr isotopic age of sphalerite from the Paoma lead-zinc deposit in Sichuan Province and its implications (in Chinese). Geol China, 37: 488–494
Liu J P, Rong Y N, Zhang S G. 2017. Mineralogy of Zn-Hg-S and Hg-Se-S series minerals in carbonate-hosted mercury deposits in western Hunan, South China. Minerals, 7: 101
Luo K, Zhou J X, Feng Y X, Uysal I T, Nguyen A, Zhao J X, Zhang J. 2020. *In situ* U-Pb dating of calcite from the South China antimony metallogenic belt. iScience, 23: 101575
Mao J W, Cheng Y B, Chen M H, Franco P. 2013. Major types and time-space distribution of Mesozoic ore deposits in South China and their geodynamic settings. Miner Depos, 48: 267–294
Marshall D J. 1988. Cathodoluminescence of Geological Materials. Boston. Unwin-Hyman. 1–146
Mason A J, Henderson G M, Vaks A. 2013. An acetic acid-based extraction protocol for the recovery of U, Th and Pb from calcium carbonates for U-(Th)-Pb geochronology. Geostand Geoanal Res, 37: 261–275
Michard A, Albarède F. 1986. The REE content of some hydrothermal fluids. Chem Geol, 55: 51–60
Nuriel P, Weinberger R, Kylander-Clark A R C, Hacker B R, Craddock J P. 2017. The onset of the Dead Sea transform based on calcite age-strain analyses. Geology, 45: 587–590
Paton C, Woodhead J D, Hellstrom J C, Hergt J M, Greig A, Maas R. 2010. Improved laser ablation U-Pb zircon geochronology through robust downhole fractionation correction. Geochem Geophys Geosyst, 11: Q0AA06
Peng J T, Hu R H, Zhao J H, Fu Y Z, Lin Y X. 2003a. Scheelite Sm-Nd dating and quartz Ar-Ar dating for Woxi Au-Sb-W deposit, western Hunan. Chin Sci Bull, 48: 2640–2646
Peng J T, Hu R Z, Burnard P G. 2003b. Samarium-neodymium isotope systematics of hydrothermal calcites from the Xikuangshan antimony deposit (Hunan, China): The potential of calcite as a geochronometer. Chem Geol, 200: 129–136
Peng J T, Hu R Z. 2001. Carbon and oxygen isotope systematics in the Xikuangshan giant antimony deposit, central Hunan. Geol Rev, 47: 34–41
Peyrotty G, Brigaud B, Martini R. 2020. $\delta^{18}O$, $\delta^{13}C$, trace elements and REE *in situ* measurements coupled with U-Pb ages to reconstruct the

diagenesis of upper triassic atoll-type carbonates from the Panthalassa Ocean. Mar Pet Geol, 120: 104520
Pi Q H, Hu R Z, Xiong B, Li Q L, Zhong R C. 2017. *In situ* SIMS U-Pb dating of hydrothermal rutile: Reliable age for the Zhesang Carlin-type gold deposit in the golden triangle region, SW China. Miner Depos, 52: 1179–1190
Pinet N, Davis W J, Petts D C, Sack P, Mercier-Langevin P, Lavoie D, Jackson S E. 2022. U-Pb vein calcite dating reveals the age of Carlin-type gold deposits of central Yukon and a contemporaneity with a regional intrusion-related metallogenic event. Econ Geol, 117: 905–922
Roberts N M W, Rasbury E T, Parrish R R, Smith C J, Horstwood M S A, Condon D J. 2017. A calcite reference material for LA-ICP-MS U-Pb geochronology. Geochem Geophys Geosyst, 18: 2807–2814
Salvi S, Williams-Jones A E. 1996. The role of hydrothermal processes in concentrating high-field strength elements in the Strange Lake peralkaline complex, northeastern Canada. Geochim Cosmochim Acta, 60: 1917–1932
Sheng X, Tang Y Y, Bi X W, Hu R Z, Xu L L, Li J, Tang Y W. 2022. *In situ* U-Pb dating of calcite indicates a Miocene Sb-Pb mineralization event in the Sanjiang base metal metallogenic belt, SW China. J Geochem Explor, 238: 107004
Shu L S. 2006. Predevonian tectonic evolution of South China: From Cathaysian block to Caledonian period folded orogenic belt (in Chinese). Geol J China Univ, 12: 418–431
Smith-Schmitz S E, Appold M S. 2018. Prediction of ore fluid metal concentrations from solid solution concentrations in ore-stage calcite: Application to the Illinois-Kentucky and Central Tennessee Mississippi Valley-type districts. Geochim Cosmochim Acta, 225: 210–227
Smith-Schmitz S E, Appold M S. 2021. Determination of fluorine concentrations in mineralizing fluids of the Hansonburg, New Mexico Ba-F-Pb district via SEM-EDS analysis of fluid inclusion decrepitates. J Geochem Explor, 230: 106861
Studemeister P A. 1984. Mercury deposits of western California: An overview. Mineral Depos, 19: 202–207
Su W C, Hu R Z, Xia B, Xia Y, Liu Y. 2009. Calcite Sm-Nd isochron age of the Shuiyindong Carlin-type gold deposit, Guizhou, China. Chem Geol, 258: 269–274
Su W C, Yang K Y, Hu R Z, Chen F. 1998. Fluid inclusion chronological study of the Carlin-type gold deposits in southwestern China: As exemplified by the Lannigou gold deposit, Guizhou province (in Chinese). Acta Mineral Sin, 18: 359–362
Sun G T, Shen N P, Su W C, Feng Y X, Zhao J X, Peng J T, Dong W D, Zhao H. 2016. Characteristics and implication of trace elements and Sr-Nd isotope geochemistry of calcites from the miaolong Au-Sb deposit, Guizhou Province, China (in Chinese). Acta Mineral Sin, 36: 404–412
Sun S S, McDonough W F. 1989. Chemical and isotopic systematics of oceanic basalts: Implications for mantle composition and processes. Geol Soc Lond Spec Publ, 42: 313–345
Tan J J, Liu C P, Yang H M, Cai Y X, Lu S S. 2018. Geochronology and Ore-Forming Material Source Constraints for Rouxianshan Pb-Zn Deposit in Huayuan Ore Concentration Area, Western Hunan. Earth Science, 43: 2438–2448
Tan Q P, Xia Y, Wang X, Xie Z J, Wei D T. 2017. Carbon-oxygen isotopes and rare earth elements as an exploration vector for Carlin-type gold deposits: A case study of the Shuiyindong gold deposit, Guizhou Province, SW China. J Asian Earth Sci, 148: 1–12
Tu G C, Gao Z M, Hu R Z, Zhang Q, Li C Y, Zhao Z H, Zhang B G. 2004. The geochemistry and ore-forming mechanism of the dispersed elements (in Chinese). Beijing: Geological Publishing House. 1–153
Uysal I T, Zhao J X, Golding S D, Lawrence M G, Glikson M, Collerson K D. 2007. Sm-Nd dating and rare-earth element tracing of calcite: Implications for fluid-flow events in the Bowen Basin, Australia. Chem Geol, 238: 63–71
Vaks A, Woodhead J, Bar-Matthews M, Ayalon A, Cliff R A, Zilberman T, Matthews A, Frumkin A. 2013. Pliocene-Pleistocene climate of the northern margin of Saharan-Arabian Desert recorded in speleothems from the Negev Desert, Israel. Earth Planet Sci Lett, 368: 88–100
Veizer J, Compston W. 1974. $^{87}Sr/^{86}Sr$ composition of seawater during the Phanerozoic. Geochim Cosmochim Acta, 38: 1461–1484
Vermeesch P. 2018. IsoplotR: A free and open toolbox for geochronology. Geosci Front, 9: 1479–1493
Wang J S, Wen H J, Shi S H. 2010. Characteristics and implications of REE, carbon and oxygen isotopes of hydrothermal calcite from the mercury metallogenic belt in Hunan and Guizhou Provinces, China (in Chinese). Acta Mineral Sin, 30: 185–193
Wang J S, Wen H J. 2015. Sm-Nd dating of hydrothermal calcites from Jiaoli-Lae Mercury deposit, Guizhou Province (in Chinese). J Jilin Univ-Earth Sci Ed, 45: 1384–1393
Wang J S. 2012. Mineralization, chronology and dynamic research of low temperature metallogenic domain, Southwest China (in Chinese). Dissertation for Doctoral Degree. Guiyang: Institute of Geochemistry, Chinese Academy of Science
Wang Q F, Yang L, Xu X J, Santosh M, Wang Y N, Wang T Y, Chen F G, Wang R X, Gao L, Liu X F, Yang S J, Zeng Y S, Chen J H, Zhang Q Z, Deng J. 2020. Multi-stage tectonics and metallogeny associated with Phanerozoic evolution of the South China Block: A holistic perspective from the Youjiang Basin. Earth-Sci Rev, 211: 103405
Wang X L, Zhou J C, Griffin W A, Wang R C, Qiu J S, O'reilly S Y, Xu X S, Liu X M, Zhang G L. 2007. Detrital zircon geochronology of Precambrian basement sequences in the Jiangnan orogen: Dating the assembly of the Yangtze and Cathaysia Blocks. Precambrian Res, 159: 117–131
Wang Y L, Chen Y C, Wang D H, Xu J, Chen Z H. 2012. Scheelite Sm-Nd dating of the Zhazixi W-Sb deposit in Hunan and its geological significance. Geol China, 39: 1339–1344
Wang Z P. 2013. Genesis and dynamic mechanism of the epithermal ore deposits, SW Guizhou, China—A case study of gold and antimony deposits (in Chinese). Dissertation for Doctoral Degree. Guiyang: Institute of Geochemistry, Chinese Academy of Science
Wei H T, Shao Y J, Ye Z, Xiong Y Q, Zhou H D, Xie Y L. 2017. REE and Sr isotope geochemistry of gangue calcites from Huayuan Pb-Zn orefield in western Hunan, China (in Chinese). Chin J Nonferrous Metals, 27: 2329–2339
Wu S, Yang Y, Roberts N M W, Yang M, Wang H, Lan Z, Xie B, Li T, Xu L, Huang C, Xie L, Yang J, Wu F. 2022. *In situ* calcite U-Pb geochronology by high-sensitivity single-collector LA-SF-ICP-MS. Sci China Earth Sci, 65: 1146–1160
Xiao X G. 2014. Geochronlogy, ore geochemistry, and genesis of the Banpo antimony deposit, Guizhou Province, China (in Chinese). Dissertation for Doctoral Degree. Kunming: Kunming University of Science and Technology
Xie Z J, Xia Y, Cline J S, Yan B W, Wang Z P, Tan Q P, Wei D T. 2017. Comparison of the native antimony-bearing Paiting gold deposit, Guizhou Province, China, with Carlin-type gold deposits, Nevada, USA. Miner Depos, 52: 69–84
Xiong S F, Gong Y J, Jiang S Y, Zhang X J, Li Q, Zeng G P. 2018. Ore genesis of the Wusihe carbonate-hosted Zn-Pb deposit in the Dadu River Valley district, Yangtze Block, SW China: Evidence from ore geology, S-Pb isotopes, and sphalerite Rb-Sr dating. Miner Depos, 53: 967–979
Xiong S F, Jiang S Y, Chen Z H, Zhao J X, Ma Y, Zhang D, Duan Z P, Niu P P, Xu Y M. 2022. A Mississippi Valley-type Zn-Pb mineralizing system in South China constrained by *in situ* U-Pb dating of carbonates and barite and *in situ* S-Sr-Pb isotopes. GSA Bull, 134: 2880–2890
Xu J W, Liu X H, Lai J Q, He H S, Song X F, Zhai D G, Lin B, Wang Y H, Shi J, Zhou X. 2022. *In situ* U-Pb geochronology of calcite from the world's largest antimony deposit at Xikuangshan, Southern China. Minerals, 12: 899
Yan D P, Zhou M F, Song H L, Wang X W, Malpas J. 2003. Origin and tectonic significance of a Mesozoic multi-layer over-thrust system within the Yangtze Block (South China). Tectonophysics, 361: 239–254
Yang H M, Liu C P, Duan R C, Gu X M, Lu S S, Tan J J, Cai Y X, Zhang L G, Qiu X F. 2016. Rb-Sr and Sm-Nd isochron ages of Bokouchang Pb-Zn deposit in Tongren, Guizhou Province and their geological im-

plication (in Chinese). Geotect Metal, 39: 855–865
Yang Q, Liu W H, Zhang J, Wang J, Zhang X J. 2019. Formation of Pb-Zn deposits in the Sichuan-Yunnan-Guizhou triangle linked to the Youjiang foreland basin: Evidence from Rb-Sr age and *in situ* sulfur isotope analysis of the Maoping Pb-Zn deposit in northeastern Yunnan Province, southeast China. Ore Geol Rev, 107: 780–800
Yang T, Duan Q F, Tian W. 2014. Geological characteristics and prospecting potential of Chatian Pb-Zn-Hg deposit, western Hunan province (in Chinese). Geol Miner Resour South China, 30: 109–117
Yu Y S, Liu A S, Dai P Y, Zhao W Q, Tao M, Liu C P. 2017. The metallogenic epoch and ore-forming material source of the Tangbian Pb-Zn deposit in Tongren, Guizhou Province: Evidence from Rb-Sr dating of sphalerites and S-Pb isotope (in Chinese). Geol Bull China, 36: 885–892
Zhang J W, Ye T P, Dai Y R, Chen J S, Zhang H, Dai C G, Yuan G H, Jiang K Y. 2019. Provenance and tectonic setting transition as recorded in the Neoproterozoic strata, western Jiangnan Orogen: Implications for South China within Rodinia. Geosci Front, 10: 1823–1839
Zhang T Y, Li C Y, Sun S J, Hao X L. 2020. Geochemical characteristics of antimony and genesis of antimony deposits in South China (in Chinese). Acta Petrol Sin, 36: 44–54
Zhang Y X, Wu Y, Tian G, Shen L, Zhou Y M, Dong W W, Zeng R, Yang X C, Zhang C Q. 2014. Mineralization age and the source of ore-forming material at Lehong Pb-Zn deposit, Yunnan Province: Constraints from Rb-Sr and S isotopes system (in Chinese). Acta Mineral Sin, 34: 305–311
Zhang Z Z, Gong Y J, Jin S C, Qi S L, Gan J M, Zhang L G. 2018. Sm-Nd isochron age of the Dazhuyuan fluorite deposit in northeastern Guizhou and its geological significance (in Chinese). Acta Petgol Mineral, 37: 949–958
Zhao J H, Zhou M F, Yan D P, Zheng J P, Li J W. 2011. Reappraisal of the ages of Neoproterozoic strata in South China: No connection with the Grenvillian orogeny. Geology, 39: 299–302
Zhou J X, Bai J H, Huang Z L, Zhu D, Yan Z F, Lv Z C. 2015. Geology, isotope geochemistry and geochronology of the Jinshachang carbonate-hosted Pb-Zn deposit, southwest China. J Asian Earth Sci, 98: 272–284
Zhou J X, Huang Z L, Zhou M F, Li X B, Jin Z G. 2013. Constraints of C-O-S-Pb isotope compositions and Rb-Sr isotopic age on the origin of the Tianqiao carbonate-hosted Pb-Zn deposit, SW China. Ore Geol Rev, 53: 77–92
Zhou J X, Xiang Z Z, Zhou M F, Feng Y X, Luo K, Huang Z L, Wu T. 2018. The giant Upper Yangtze Pb-Zn province in SW China: Reviews, new advances and a new genetic model. J Asian Earth Sci, 154: 280–315
Zhou M F, Yan D P, Kennedy A K, Li Y Q, Ding J. 2002. SHRIMP U-Pb zircon geochronological and geochemical evidence for Neoproterozoic arc-magmatism along the western margin of the Yangtze Block, South China. Earth Planet Sci Lett, 196: 51–67
Zhou Y, Duan Q F, Chen Y C, Tang J X, Cao L, Gan J M. 2015. Rb-Sr dating and tracer study of quartz from the Jiangjiaya lead-zinc deposit in western Hunan (in Chinese). Geol China, 42: 597–606
Zhu J J, Hu R Z, Richards J P, Bi X W, Stern R, Lu G. 2017. No genetic link between Late Cretaceous felsic dikes and Carlin-type Au deposits in the Youjiang basin, Southwest China. Ore Geol Rev, 84: 328–337
Zou H, Li M, Santosh M, Zheng D, Cao H W, Jiang X W, Chen H F, Li Z Q. 2022. Fault-controlled carbonate-hosted barite-fluorite mineral systems: The Shuanghe deposit, Yangtze Block, South China. Gondwana Res, 101: 26–43

(Responsible editor: Jianwei LI)